Nerve Pathways with MR Tractography

8

Maria Eugenia Caligiuri, Andrea Cherubini, Carlo Cosentino, Francesco Amato, Tommaso Scarabino, and Umberto Sabatini

The neuroradiological interpretation of magnetic resonance (MR) images relies on a complex semeiotics that is based on the morphological and signal characteristics of normal and pathological brain tissue and on the detailed knowledge of the ultrastructural and functional organization of the central nervous system (CNS). In the brain, the study of cortical organization is facilitated by the presence on its surface of fissures, which divide it into lobes, and sulci, which circumscribe in each lobe a number of convolutions or gyri. Identification of subcortical nuclei, grey matter formations lying deep in the hemispheres, is also facilitated by their characteristic morphology, their symmetric position with respect to the midline and the presence of well-defined white matter structures such as the internal, external and extreme capsule that mark their borders.

Detailed evaluation of white matter structure is more challenging than the study of cortical organization, because it does not exhibit anatomical landmarks except the contiguous cortical gyri, the ventricular systems and the base nuclei; however, white matter contains fibres with distinct anatomical courses and functional significance that include projection, association and commissural systems. Identification of nerve fibre bundles is essential in neurophysiology and in studying CNS diseases. Furthermore, knowledge of the spatial relationship between fibres and lesions requiring surgical treatment is crucial in order to preserve white matter functional pathways and the activities they promote.

Conventional and morphometric MR techniques provide an accurate representation of the brain's macroscopic anatomy, but they do not carry detailed information on white matter structure. By contrast, the study of the anisotropic diffusion of water molecules (diffusion tensor imaging; DTI) [1] and tractography (fibre tracking) provide data on white matter microscopic organization and allow the reconstruction of axonal tracts using diffusion-weighted MR images [2–6]. Since tractography is currently the sole

M.E. Caligiuri • A. Cherubini
Institute of Molecular Bioimaging and Physiology of the National Research Council (IBFM-CNR), Catanzaro, Italy

C. Cosentino • F. Amato
Faculty of Biomedical Engineering, Magna Graecia University, Catanzaro, Italy

T. Scarabino
Department of Radiology and Neuroradiology, PO "L. Bonomo" Hospital, Andria (BT), Italy

U. Sabatini (✉)
Institute of Neuroradiology, Magna Graecia University, Catanzaro, Italy
e-mail: u.sabatini@hsantalucia.it

T. Scarabino et al. (eds.), *High Field Brain MRI*, DOI 10.1007/978-3-319-44174-0_8

method affording non-invasive study of the 3D architecture of axons in vivo, it has potential applications to several fields of neurology and neurophysiology to visualize and quantify physiological mechanisms and pathological processes.

Herein we illustrate the main methods for modelling diffusion-weighted MR images and for performing tractography and discuss their enormous potential and current limitations.

8.1 Basic Principles

A brief overview of the structural characteristics of nerve tissue is helpful for understanding the rationale behind diffusion studies. While grey matter is made up of cells, principally neuronal soma, white matter is mainly composed of myelinated axons with a specific orientation. Axons have a mean diameter of ~20 μm and may form parallel bundles of varying thickness.

The rationale behind DTI and tractography is that the random movement of water molecules in tissues (diffusion) is restricted by the presence of cell structures (Fig. 8.1). As a consequence, diffusion perpendicular to axon bundles is hindered by axonal cell membranes and myelin sheaths [7, 8] whereas it is unrestricted along them. Within axons water is surrounded by cell membranes and myelin sheaths; again, its diffusion will be greater parallel to the fibres. Longitudinally oriented axoplasmic neurofilaments do not seem to restrict diffusion [9]. Tissues like cerebral white matter, which possess a microscopic architecture characterized by a specific spatial orientation, will thus exhibit different diffusion values in the different spatial directions. When diffusion exhibits a preferential direction, it is termed anisotropic.

The diffusion of water molecules in biological tissues can be measured using MR gradients and diffusion-weighted sequences. The acquisition technique consists of "tagging" the water molecules with a very short gradient. Tagged molecules acquire a magnetization and a phase that depend on their spatial position. The natural phenomenon of diffusion causes the displacement of these molecules to areas containing molecules with different magnetization and phase. The presence in a region of signals with different magnetization and phase results in an overall lower signal intensity, as the signal of the diffusing molecules reduces the one of local molecules. Therefore, increasing diffusion of the water molecules induces a reduction in tissue signal. The study of diffusion anisotropy uses the same image

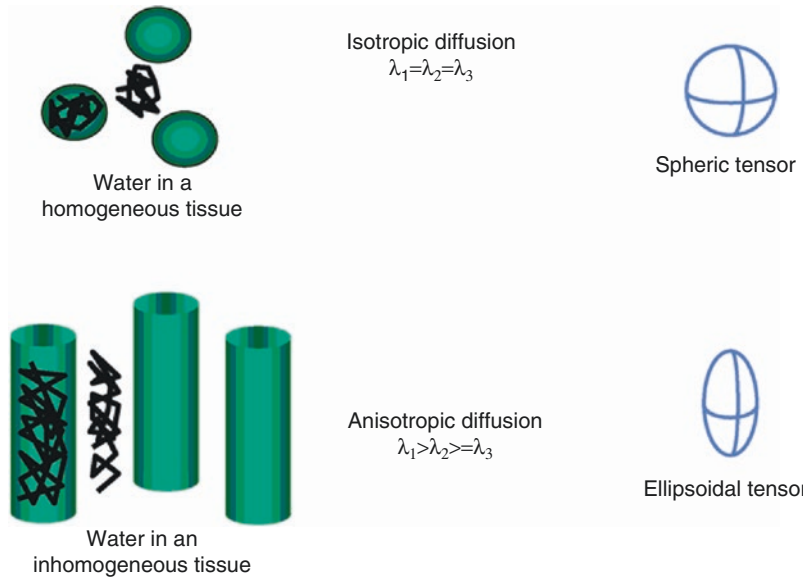

Fig. 8.1 Representation of the physical bases of the reconstruction of the diffusion tensor. In homogeneous tissues, the three eigenvalues have similar values, and the tensor is spherical. In tissues where barriers restrict water diffusion in a particular direction, the tensor is an ellipsoid, and the direction corresponding to the principal eigenvalue represents the direction of the fibres

acquisition strategies as clinical diffusion studies. Indeed, water molecule diffusion data are actually generated as anisotropic data, because all acquisitions read diffusion along a given spatial direction, coinciding with the direction of the magnetic field gradient used. In clinical diffusion studies, the direction information is lost through the averaging of diffusion values along the three spatial axes; this simplifies the detection of pathological changes in the diffusion coefficient, which are independent of fibre direction.

In DTI studies, this information is retained, and the prevalence of diffusion along a direction, e.g. along a fibre bundle, can be expressed in terms of anisotropy. The degree of anisotropy can be quantified using the diffusion tensor [9–11]. A tensor is a complex mathematical entity [12]; when measured with MR, it may be represented in matrix form using data from diffusion-weighted images to obtain parameters like fractional anisotropy (FA) and the apparent diffusion coefficient (ADC), better known nowadays as mean diffusivity (MD) [13]. The diffusion tensor also contains much additional information. In particular, an algebraic procedure called diagonalization makes it possible to obtain for each image voxel three eigenvalues (λ_1, λ_2, λ_3) representing the values of diffusion along three spatial directions (eigenvectors). If in a given voxel the three values are similar ($\lambda_1 \sim \lambda_2 \sim \lambda_3$), as in all grey matter, the water diffuses in a similar manner in all directions and its diffusion in the voxel is called isotropic. If, by contrast, one of the three eigenvalues is much greater than the other two, as in white matter, water diffuses more easily along the direction corresponding to that eigenvalue, and its diffusion in the voxel is anisotropic.

It is worth noting that, unlike MR parameters such as relaxation times, those obtained from the diffusion tensor do not depend directly on the magnetic field and can thus be measured and directly compared between high- and low-field acquisitions. In practice, whereas T1 and T2, and thus the relevant images, change as a function of the magnetic field, water diffusion in a given space is the same at 1.5, 3.0 and even 7.0 T. Diffusion studies thus fully benefit from the greater signal/noise ratio (SNR) of high-field magnets.

8.2 Image Acquisition

Calculation of the diffusion tensor requires acquisition of a set of MR images using suitable diffusion-weighted sequences. Echo-planar sequences with different gradient directions and intensities are the more appropriate for these applications and are those most commonly used [1, 14, 15].

Diffusion weighting involves a general reduction in signal intensity, which increases the greater the diffusion of water. This magnifies the SNR problems shared by all MR acquisitions and makes it difficult to obtain images with very high spatial resolution. Currently, the best spatial resolution that can be achieved is rarely less than 1 mm, particularly along the slice-encoding direction, but the use of high magnetic fields (3.0 T or greater) and parallel imaging can further enhance resolution [16]. Diffusion weighting depends on gradient intensity, which is usually denominated *b* factor and is measured in s/mm^2. In theory, increasing *b* values should be used to calculate MD; in practice, limitations in the gradients used in clinical practice, specific absorption rate and times of acquisition have led to the prevalent use of only two *b* values, one virtually null (no diffusion weighting) and the second high (1000 s/mm^2 or greater). A *b* value slightly greater than 0 (~20) is used to remove the effects of large vessels. The minimum set of images to be acquired for a DTI study includes six different diffusion-weighted directions (with $b = 1000$ or greater) and a non-diffusion-weighted scan ($b = 0$). The minimum set may be acquired several times to improve the SNR, whereas acquisitions with different *b* values for each direction are unnecessary as well as inefficient in terms of SNR [11]. More accurate evaluation of the diffusion coefficient *D* from two acquisitions has been demonstrated using two values of *b* differing by ~1/*D*, which in the brain entails that $b2–b1 <$ 1000–1500 s/mm^2 [11, 17]. If more than two acquisitions are performed to optimize the SNR,

the theory of error propagation states that it is more convenient to obtain multiple acquisitions at the two *b* values selected than to use a broader range of *b* values [11].

Acquisitions of *b* values in a range, rather than a pair ($b = 0$ and $b = 1000$), can however provide interesting information [18, 19]. Although a single MD value is usually assigned at each tissue voxel, most tissues are indeed made up of separate compartments, each bearing its distinct value of MD. Brain tissue comprises at least two compartments, a fast-diffusion intracellular compartment and a slower-diffusion extracellular compartment. The MD depends on the range of *b* values used, because low values (1000) are more sensitive to fast-diffusion components and thus to the structural features of the interstitium, than to those of axon fibres. Ideally, the different tissue compartments should be studied separately using several different *b* values and then fitted with a multi-exponential function. However, since slow-diffusion compartments can be studied only with high *b* values and favourable SNRs, this is difficult to achieve.

Simulation studies [20] confirmed the notion that higher *b* values allow the attainment of shaper angular diffusion profiles, which are more sensitive to the orientation of fibres. In particular, by increasing the *b* value from 1000 to 3000 s/mm^2, the minimal resolvable angle between fibre bundles was reduced from about 45 to 30°, independently from the number of diffusion-encoding gradient orientations. Instead, increasing the *b* value to 5000 s/mm^2 did not improve the diffusion model further.

The number of directions offering the best compromise between a reliably reconstructed tensor (multiple directions) and long acquisition times is still debated. In a given voxel, if the fibres are all oriented along the same axis, sampling of the angular diffusion space along a limited set of directions (at least six) is not a problem. However, large portions of white matter are characterized by complex fibre configurations [21], and for this reason the diffusion-weighted signal needs to be acquired along a larger number of unique orientations in order to obtain an accurate reconstruction of fibre orientation distribution functions. Even in the case of a single direction of the fibres within a voxel, a high number of sampling directions would be needed, since the orientation of this direction might change from voxel to voxel.

Besides increasing the precision (reproducibility) in reconstructing fibre orientation distribution functions, a higher number of unique sampling orientations will also reduce the extent to which the variance in an estimate of a given parameter depends on the orientation of the structure. For example, while from a mathematical standpoint at least six different directions plus a low *b* value acquisition are required in order to fit the diffusion tensor model, it has been shown that for a statistically rotationally invariant reconstruction (such that the variance in tensor-derived parameters is independent of the orientation of the tensor) at least 30 directions uniformly distributed over the sphere are needed [22]. Currently, most researchers use 6 to 90 different directions, with considerable differences in acquisition times and uncertain benefit. A sequence with 68 directions, $b = 100$ and 1000 s/mm^2, and a cubic voxel of 2.3 mm lasts about 13 min, but actually takes much longer because image averaging to obtain an acceptable SNR requires multiple acquisitions. Here, a large role is played by acquisition conditions, particularly magnetic field intensity and the availability of parallel imaging to improve the SNR.

High-angular resolution techniques (HARDI; [23]), which require a much greater number of directions (even 252 or more), benefit from favourable conditions of field intensity and high coil sensitivity. A drawback of HARDI techniques is their requirement for a greater number of diffusion-encoded acquisitions compared to DTI, leading to an increase in acquisition time. In addition, these techniques often use a substantial amount of the acquisition sequence duration for the diffusion-encoding gradients, resulting in long repetition and scan times. For example, a typical 60-direction, 60-slice whole-brain Q-ball acquisition can take up to 10 min to complete the diffusion and slice encoding, while a 257-direction whole-brain diffusion spectrum imaging scan lasts as long as 45 min. The length

of these acquisitions limits their utility in clinical and research studies. In order to overcome this limitation, several approaches have been developed, such as conventional accelerated 2D parallel imaging approaches and simultaneous multi-slice approaches for single-shot echo-planar imaging. With 2D parallel imaging [24], the number of phase-encoding steps can be decreased by a factor up to 4, thus significantly reducing image distortion and blurring. Despite allowing for an improved image quality, this reduction in echo train length does not translate to a significant reduction in acquisition time because of the large fixed diffusion-encoding time blocks [25]. On the other hand, multi-slice approaches can reduce scan time by a factor equal to the number of excited slices, which are diffusion-encoded with the same diffusion gradients, and readout simultaneously. Methods developed according to this approach include wideband imaging [26, 27], simultaneous image refocusing (SIR) [28, 29] and parallel image reconstruction-based multi-slice imaging [30–34]. Unfortunately, these techniques suffer from significant artefact and/or SNR loss: the wideband approach suffers from a large voxel tilting artefact, while the SIR technique necessarily lengthens the readout period of the echo-planar imaging, thus increasing echo time and susceptibility-induced image distortions. On the other hand, multi-slice imaging techniques based on parallel image reconstruction can lead to a large SNR penalty related to the g-factor, since the aliased slices are generally close to each other due to a comparatively small field of view (FOV) in the slice direction. Several attempts have been developed to solve these issues, such as the controlled aliasing in parallel imaging results in higher acceleration (CAIPIRINHA) technique [30] and the blipped-CAIPI method [34].

As mentioned above, the diffusion tensor basically provides two types of information: a quantitative estimate of diffusion anisotropy and the spatial orientation of fibres (Fig. 8.2). These data are interesting but "local", i.e. they regard a single voxel. Tractography uses these microscopic data to obtain "global" information and reconstruct macroscopic fibre tracts.

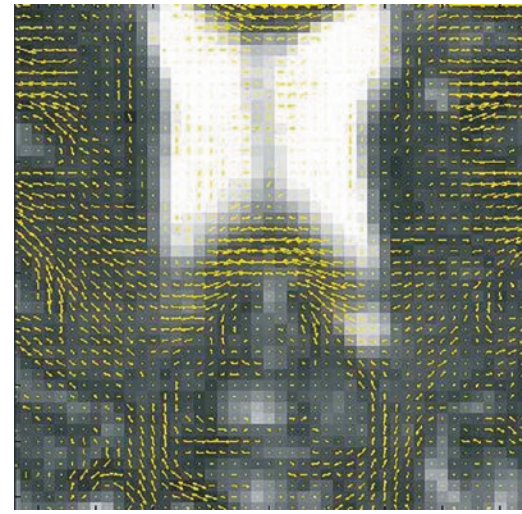

Fig. 8.2 Diffusion tensor. Projection in the image plane of the principal eigenvector. Vectors are represented by *double-headed arrows* because diffusion data provide the direction, not the orientation of diffusion

8.3 Fibre-Tracking Techniques

8.3.1 Line Propagation Algorithm: Deterministic Tractography

The voxel grid of an MR image may be compared to a chessboard: selecting a number of adjacent voxels that form a trajectory is like drawing a line on the chessboard (Fig. 8.3). The algorithm used to draw this trajectory in most fibre-tracking techniques involves selecting an initial point (seed point) that is highlighted on the image and then moving to the next nearest voxel, which in turn is highlighted, along the prevalent anisotropic direction, until a condition that halts this process arises (stopping criterion). The differences among these, line propagation, algorithms lie in the way in which the information contained in the voxels nearest to the one being examined with the algorithm (nearest neighbours approach) is used by the algorithm itself to draw the likeliest trajectories and minimize noise.

Since digital images are represented on discrete fields, the vector will often point to an area straddling at least two adjacent voxels, requiring a choice from one or more possible trajectories. In such cases, the selected tract will be a mere

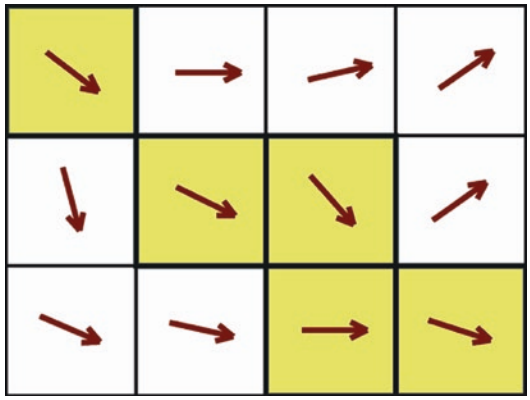

Fig. 8.3 Propagation of a fibre in a vector field. The *yellow pixels* represent the course of the reconstructed fibre

approximation of the information contained in the diffusion data, irrespective of the trajectory that has been selected.

The first researchers to reconstruct a white matter fibre tract successfully [35, 36] solved this problem using propagation in a continuous numerical field – where the coordinates can be expressed as decimal values – each time approximating the coordinates of the line to those of the nearest voxel. This simple but fairly rough method can be improved by applying a tract curvature threshold. Assuming that the course of a fibre tract exhibits only reasonably soft curves, whenever two possible trajectories present, the less curved one is selected, while sharp curves (e.g. >60°) are excluded. Line propagation algorithms may require vector interpolation (direction and eigenvalue) at the point of arrival of the previous step, which usually straddles two or more voxels and therefore does not directly correspond to a measured value. Interpolation is a mathematical operation that makes it possible to obtain the value of a point from those of surrounding points. In the simpler algorithms, the vectors corresponding to the neighbouring voxels are interpolated, while the more sophisticated ones directly interpolate the diffusion tensor and calculate a new vector [6]. Interpolation enables more uniform paths to be obtained with respect to the algorithms that do not employ them and is less sensitive to noise, although the additional calculations considerably increase computation time.

8.3.2 Global Algorithms

The algorithms of this class use a radically different approach. In fact, whereas the line propagation algorithms use only local information (i.e. the data contained in a voxel and in those nearest to it), these techniques employ the information in a global way by applying a mathematical function that reproduces the structural characteristics of the fibre tracts. For instance, the physical analogy used for the fast marching technique [37–39] is that of an ink drop falling on adsorbent tissue. The stain extends faster along the direction of the tissue fibres than perpendicular to them. Assuming a vector field indicating the directions in which the ink spreads, a speed function for front propagation can be defined on the basis of the fibres' anisotropy value. This function reflects the fact that propagation is fastest along fibres and slowest perpendicular to them and makes it possible to calculate the "shape" of the stain from any point at any given time. Its contours may be compared to the isobars of meteorological charts and, in the case of a vector field of DTI data, they represent a sort of map of the likelihood of connection starting from a given point. Using this technique, the course of the fibres coincides with the faster route, hence its name.

Another physical analogy, well known in the field of numerical simulations as the "travelling salesman problem", can help explain another class of methods. A travelling salesman needs to find the optimum route passing through all the towns where he will be calling. One solution is to define a function, e.g. petrol consumption or time, and find the route that minimizes it. Using DTI data, the function ensuring global energy minimization is related to paths along the direction of the field vectors, while those associated with greater energy expenditure are perpendicular to them [40]. Calculation of the value of the function for all possible trajectories makes it possible to identify the course that minimizes the energy function. However, methods like simulated annealing allow the solution to be found rapidly without calculating the energy for all the possible courses while minimizing the effect of noise.

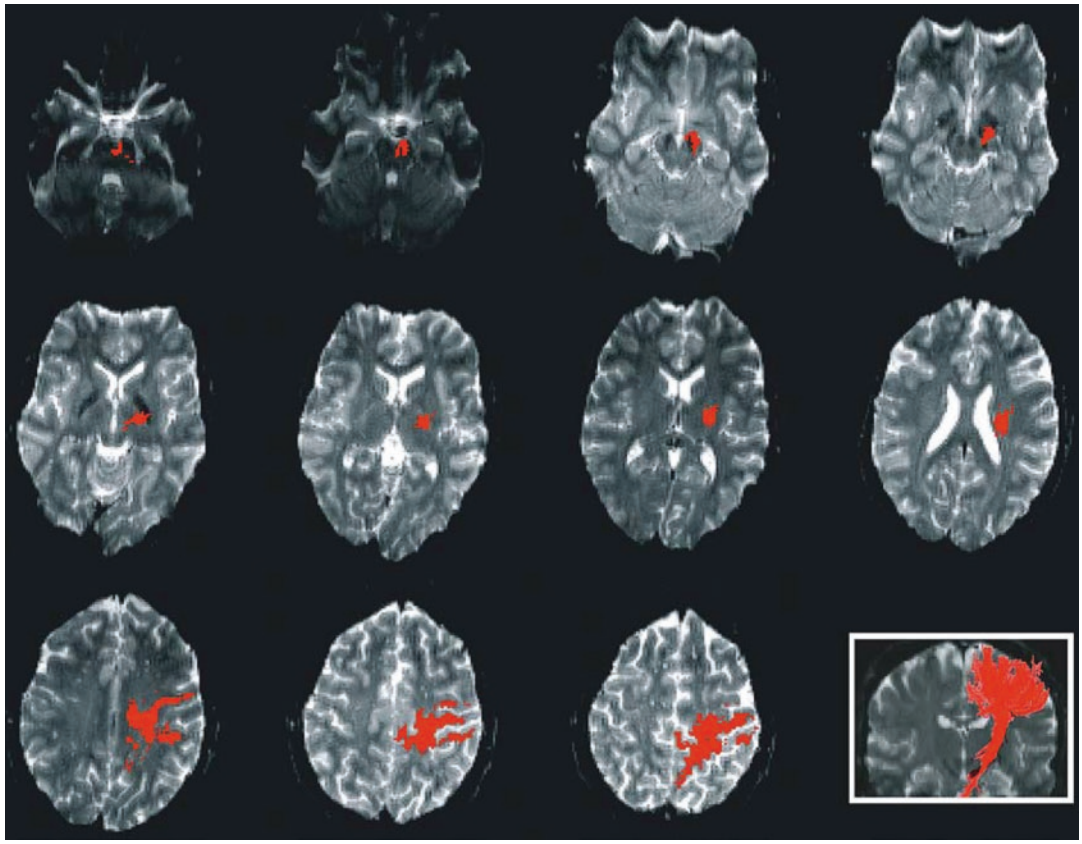

Fig. 8.4 Fibre reconstruction with a line propagation algorithm (left pyramidal tract in *red*), superimposed on axial T2-weighted images. *Lower right corner:* 3D reconstruction of the same tract overlaid on a coronal image

Global methods have two main advantages. First, they can provide a semi-quantitative estimate of the level of connectivity between two points or regions. In fact, fibres like those shown in Fig. 8.4 provide a visual representation of the bundles, but not a "value" of the connection [41], for instance, between two activation areas shown on functional MR. Secondly, they are less affected by the typical limitations of line propagation algorithms (addressed below). However, the level of calculation required to implement them is often close to the computational capacity of current processors, and they are still in an early phase of development compared with the more common line propagation algorithms (Fig. 8.5).

Halfway between deterministic (line propagation) and global algorithms are the Monte Carlo probabilistic methods [42–44]. With these techniques, thus named for their similarity to gambling, each time the tract is propagated from one voxel to the next, the various directions are given a probability value depending on the diffusion values measured. It is assumed that by repeating the line propagation a large number of times, the course that has been selected most often will correspond to the actual trajectory of the fibre.

To date, several deterministic (line propagation) and probabilistic tractography algorithms have been developed, some of which can be applied not only to DTI data but also on orientation distribution functions reconstructed on HARDI data. The most commonly used deterministic algorithm is the "fibre assignment by continuous tracking" (FACT; [36]), which is computationally leaner and requires minutes to perform whole-brain tractography for a single

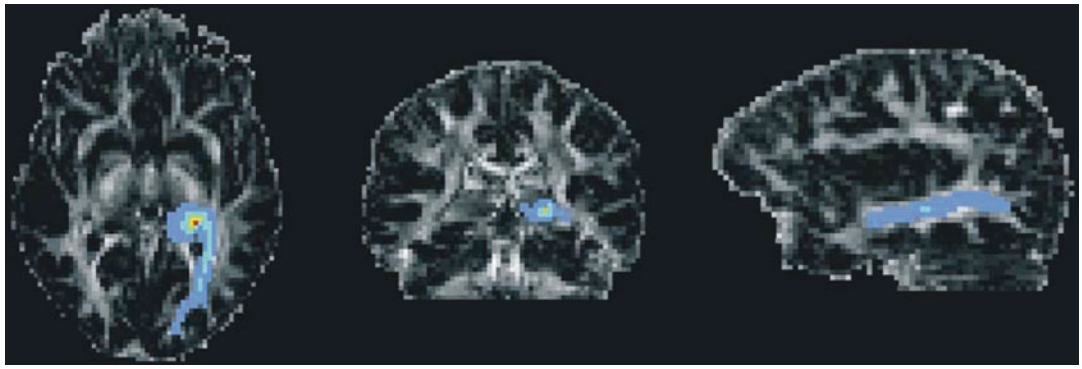

Fig. 8.5 Connectivity map generated using a Monte Carlo algorithm. Overlay on a fractional anisotropy map. Fractional anisotropy is derived from the diffusion tensor and represents white matter distribution. Colours represent the likelihood of connection with the seed point in the left lateral geniculate nucleus, according to an intensity scale

subject. For what concerns probabilistic tractography, the most commonly used approach relies on the combination of two steps [44, 45]: first, a Bayesian method for assessing the most appropriate number of fibre orientations at each voxel is performed; subsequently, probabilistic tractography through the complex orientation fields is carried out. The main advantage of this approach is that the Bayesian step allows the modelling of crossing fibres, which makes this approach more sensitive to secondary or subordinate pathways. Each voxel is modelled as an isotropic compartment (ball: "round" tensor with all eigenvalues equal) and one or several anisotropic compartments (sticks: "thin" tensors with only one non-zero eigenvalue).

However, the obtainable accuracy in identifying complex fibre configurations based on DTI data is limited [21], and HARDI approaches might be more suitable to this scope, even if their application in clinical routine is heavily limited by the long acquisition times.

8.3.3 Seed Point

A factor requiring careful consideration is the initial point of tract propagation, as this choice influences the relative effect of noise on the propagation itself. In the earliest approaches, a frequently adopted solution was to use a number of equidistant seed points arranged on a grid space. This reduced the variance connected with the arbitrary choice of the seed point. An acceptance criterion was applied to avoid selecting voxels not containing fibres. To date, the most frequently used condition is a minimum FA value ensuring the presence of a distinct fibre at the seed point. It is worth stressing that, since the directions identified in each voxel by the diffusion tensor do not have an orientation (see Fig. 8.2), a forward and a backward pathway, lying on the same straight line but running in opposite directions, are consistently generated at seed points.

More recently, because of the development of reliable brain atlases of cortical, subcortical and white matter structures, the definition of seed points has changed. In fact, by using these templates, cortical and subcortical region of interest can be automatically identified on the individual MR scan and used as seeds for tract reconstruction.

8.3.4 Stopping Criteria

All fibre-tracking algorithms that use a seed point require a stopping criterion to terminate the propagation process. The most intuitive criterion is the FA value itself; in grey matter FA is low (0.1–0.2 on a 0–1 scale), so the orientation of the

principal eigenvector of the diffusion tensor is random and unrelated to that of the fibre tract. A useful stopping criterion may thus be an FA threshold (usually 0.2) below which the propagation is halted, preventing reconstruction of fibres that are not organized into bundles, like grey matter fibres. However, this criterion may also halt the elongation of a line in those white matter voxels, which, albeit containing fibre tracts, have a low FA because of the lack of a main direction (see below).

Another possible stopping criterion is the curvature of the reconstructed fibre tract. The method used to calculate the diffusion tensor assumes the absence in the voxels of sharp curves, in line with the fundamental hypothesis of the Gaussian nature of the diffusion process in all directions. A criterion halting tract propagation in the presence of sharp angles is thus useful, but is difficult to apply to the shorter and more tortuous tracts, where the low spatial resolution of the image does not enable reconstruction of the real course of the fibres.

8.3.5 Waypoints and Termination Points

When one is interested in using tractography to reconstruct a specific white matter tract, the definition of the seed region alone might not be sufficient. In fact, no tractography algorithm, to date, directly incorporates knowledge on the actual bundles known to connect different regions of the brain, and for this reason erroneous connections might be identified. To account for this limitation, there are two main approaches, both relying on the use of atlases. A frequently used procedure is that of defining not only the starting point (seed), but also a termination region, where the tract of interest is known to have one of its ends, and, eventually, one or more regions where the tract is known to pass (waypoints). These regions may be easily identified on existing MRI atlases (see Fig. 8.6, second row). If a deterministic or probabilistic streamline crosses the waypoints (eventually in a fixed order), it will be retained for the final reconstruction of the tract, otherwise it will be excluded. Of course, also one or more avoidance masks can be defined, implying that if a streamline reaches any of their voxels, it is rejected. Waypoints, avoidance and termination regions have been successfully used in order to create an atlas of the principal fibre bundles of the human brain [47].

The second approach is mainly used in whole-brain tractography (see Fig. 8.6, third row), either deterministic or probabilistic, and consists in automatically assigning each tractography streamline to a specific white matter bundle. This labelling process relies on the correspondence of the anatomical position of the streamline with that of the white matter tracts in an atlas (which in turn could have been constructed using waypoints and termination masks).

8.3.6 Tractography-Based Metrics

The ultimate aim of tractography is, of course, to extract quantitative information regarding the brain's structural connections. To this end, there are several metrics that can be extracted from tractography data.

If deterministic tractography is performed, the exact number of streamlines that connect two regions can be calculated and, for example, compared across groups. On the other hand, if probabilistic tractography is used, an analogue measure is calculated, at each voxel, as the fraction of retained streamlines passing through the voxels over all the streamlines generated from the seed region.

Any tractographic reconstruction, appropriately thresholded in order to exclude outliers and normalized by the total number of streamlines, can also be binarized and overlaid on other MRI sequences or maps in order to extract an average value of volume (e.g. from 3D T1-weighted scans) or diffusion metrics (e.g. FA and MD). However, after the development of white matter atlases, similar results can be achieved without performing tractography on the single subjects, but rather extracting the probabilistic map for the

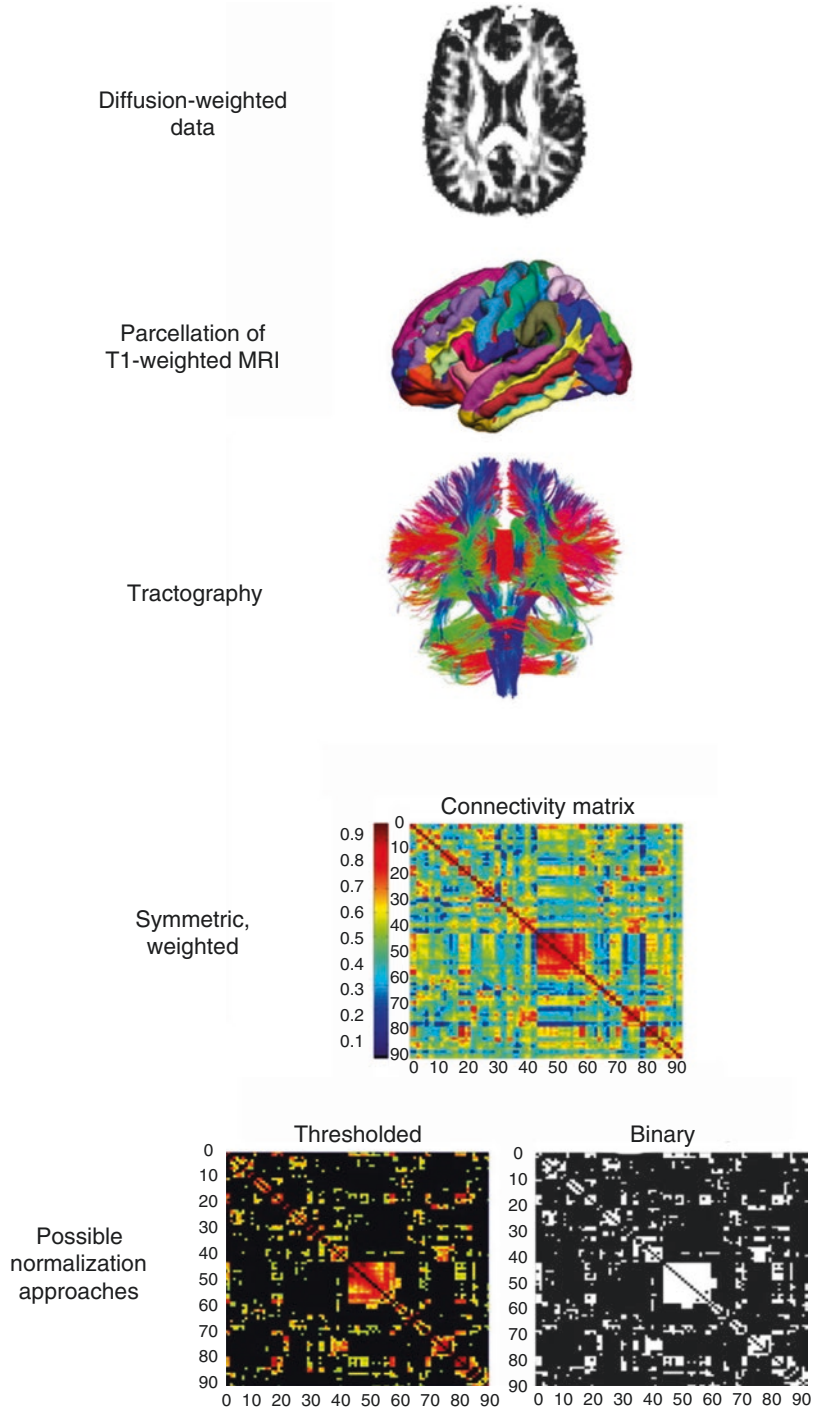

Fig. 8.6 Typical processing workflow for the reconstruction of whole-brain connectivity and network analysis (Adapted from Filippi et al. [46]). Diffusion-weighted data is used to perform tractography (*first row*). Atlas-based identification of cortical and subcortical brain regions on the individual brain (parcellation, *second row*) can be used to define seeds, targets, waypoints and exclusion masks for fibre tracking (*third row*). By using all the regions defined in the atlas to generate pairwise comparisons, a connectivity matrix is obtained in which the connection strength between all pairs of nodes is contained (*fourth row*). To obtain comparability across different subjects, a normalization step is required (*bottom row*): the matrix can be thresholded, to exclude weak connections, and or binarized, to exclude connection weights from the analysis

region of interest from the atlas itself and registering it on the subject's image.

The most recently introduced method for exploiting tractography data is represented by the application of graph theory to reconstructed fibre bundles, which is known as structural connectomics [48, 49]: this theory considers pairwise brain connections (reconstructed using any fibre-tracking method) with the scope of modelling the brain as a complex network consisting of *nodes* (i.e. regions of the cortex and subcortical nuclei) connected by *edges* (i.e. the white matter bundles). There is a large number of theoretical metrics that can be extracted from graphs in order to quantify network organizational properties both at the global and the local. Here we briefly describe the metrics most frequently used in neuroimaging studies that exploit brain graph analysis [50]. The node *degree* is the number of edges connected to a given node. For each node, the *clustering coefficient* is defined as the ratio of the number of actual connections among the first-degree neighbours to the number of all possible connections. The clustering coefficient indicates the extent to which neighbouring nodes are interconnected to one another, thus reflecting the local efficiency of information transfer of a network. In order to assess the graph distance between nodes, the *shortest path length* is computed by counting the minimum number of edges needed to link any node pair. To measure the centrality of a node (i.e. its importance with respect to the entire network), *node betweenness centrality* is computed as the fraction of all shortest paths that contain the specific node. Similarly, *edge betweenness centrality* measures how influential any given edge is with respect to the entire network and is defined as the fraction of all shortest paths in the network that contain the considered edge. At the graph global level, instead, the *characteristic path length* is calculated as the average of all the shortest path lengths (i.e. across all node pairs), while the *global efficiency*, another frequently used graph metric, is the average of all the inverse shortest path lengths. Both characteristic path length and global efficiency quantify the global integration of the network, with the latter preferred if measuring topological distances in relatively disconnected graphs. Finally, any complex network in graph theory can be decomposed into *modules*. Each module is composed by a set of nodes whose connections with each other are much stronger than their connections to nodes in different modules. To quantify the community structure, the *modularity* metric can be used to assess how strongly nodes in a community interconnect compared to a random graph with the same number of nodes and edges (i.e. a graph where the edges occur at random). Thus, modularity is a statistical quantity related to the extent to which a network is decomposable into such clearly delineated modules.

Whenever applying graph analysis to tractography data, an important aspect to consider is that intrinsic network organizations are better assessed at a specific connection density, as this way it is less influenced by intersubject variability in the total number of reconstructed streamlines. If the appropriate density were not used, each subject's raw connectivity matrix (containing, for each subject, the number of connections between any node pair, see Fig. 8.6, bottom rows) would show substantial differences in connections between regions of interest, based on slight variations in individual anatomy. To normalize the network density, connectivity matrices must be thresholded. The threshold is chosen so that a specified percentage of edges is preserved in the network. Furthermore, by imposing another threshold on edge weights (e.g. fibre density), only the strongest edges are preserved, reducing the likelihood of including spurious connections not supported by evidence [51]. Normalized networks allow for topological properties such as path length and clustering to be quantitatively compared across subjects. Binarization of edges aids this process by ensuring that in addition to the number of edges being identical across subjects, the sum of edge weights is also identical. In recent years, several studies used graph theory to explore the organization of brain circuits in healthy controls and different populations of patients with neurological and psychiatric disorders [46, 52–55].

8.4 Limitations of Tractography Techniques and Their Solutions

Also due to their recent introduction, tractography techniques suffer from a number of drawbacks.

8.4.1 Noise

Owing to the frequent need for compromising between acquisition time and image quality, the three-dimensional vector field that is obtained using DTI data may contain a high level of noise. Several researchers have tried to quantify the effects of noise on tensor and tract reconstruction [56–61]. Unlike what takes place in standard MR, the noise present in the reconstructed tensor is not directly perceived on images like those of Figs. 8.2 and 8.4, because it affects only the direction of the tracts. Consequently, though exhibiting a consistent distribution of directions, the vectors may indicate slightly different trajectories with respect to the actual anatomy. This type of noise considerably affects fibre tracking, and one of the main problems of line propagation algorithms is that such errors accumulate with increasing distance from the seed point [44]. Therefore, the greater this distance, the higher the risk of deviation of the reconstructed fibre towards an adjacent, unconnected fibre tract. This possibility should always be taken into account when analysing DTI reconstructions, especially of long fibre tracts. SNR optimization is essential to obviate this and other, conceptually related problems. Here, too, the intensity of the magnetic field used and the availability of parallel imaging play a large role.

8.4.2 Partial Volume

Different types of tissue may be found in a single voxel (partial volume effects), resulting in a reduction in the value of anisotropy [62]. Partial volume effects constitute a problem for fibre-tracking techniques. The problem may be accentuated in short fibre tracts and in those close to grey matter, where white matter tends to thin out and anisotropy to diminish. Addressing partial volume effects requires spatial resolution to be increased, thus reducing the SNR. As in the previous case, the solution lies in defining the noise level tolerated by the algorithm used and in adjusting the resolution and acquisition time of the MR image.

8.4.3 Ultrastructure and Complex Fibre Configurations

DTI provides information on fibre bundles, not on individual axon branches. In addition, the diffusion tensor is unable to model adequately voxels containing more than two axon populations with different directions [63]. For instance, if the relationship among the three eigenvalues of the diffusion tensor is of the type $\lambda_1 = \lambda_2 > \lambda_3$, the FA may still be sufficiently high as to fail to halt a line propagation algorithm, even in the absence of a major direction with an eigenvalue greater than the other two. In this case, the plane defined by the *two* major eigenvectors contains several more or less equivalent directions, leading to error. This problem stems from the nature of the diffusion tensor itself, which being a mere second-order approximation of the diffusion process, cannot adequately represent complex situations like the one described. The tensor line technique partially obviates this problem by selecting, among the directions of the plane defined by the two main eigenvectors, the one minimizing the curvature of the trajectory according to the original direction [59].

These methods do not address the possibility that a dominant direction is not identified in a voxel due to crossing bundles giving rise to different directions. The inability to resolve a single direction within each voxel is a significant general limitation of DTI. In fact, in the millimetre scale of the MR voxel, voxels typically exhibit a number of fibre orientations. Common situations of intra-voxel heterogeneity of orientations may be due to the intersection of different white matter bundles or to the complex architecture of sub-

cortical or junctional fibres. In the presence of fascicles with multiple directions within the same voxel, for example, due to crossing or divergence, DTI will estimate the prevalent direction, which does not necessarily correspond to any actual direction. For instance, if in a voxel a vertical bundle branches off a horizontal bundle, DTI will show the presence of a single direction corresponding to their diagonal, thus failing to represent either.

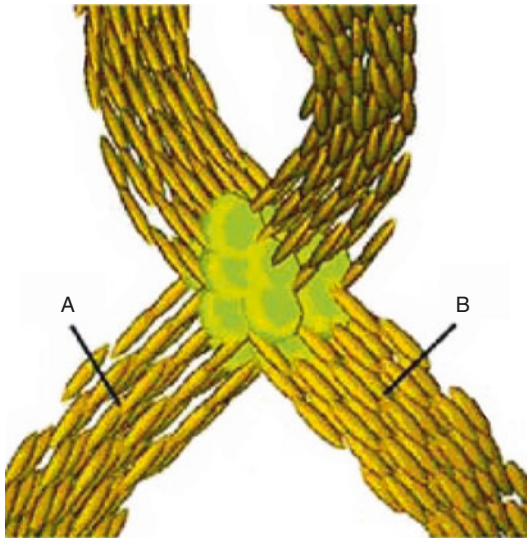

Fig. 8.7 The crossing of two fibre bundles may result in a spherical diffusion tensor, erroneously indicating an absence of fibres

The standard diffusion tensor reconstruction technique using DTI data cannot resolve this problem. Indeed, even using several different diffusion-weighting directions to reconstruct the tensor, its mathematical nature prevents it from identifying the different directions when, for instance, two or three different bundles cross. The inability of the DTI technique to resolve fibres with multiple directions derives from the assumption of the Gaussian nature of the tensor model, because a Gaussian function has a single directional peak, preventing the recognition of multidirectional diffusion by the tensor model.

Methods capable of using all the diffusion information are HARDI techniques [23], which measure diffusion in several directions with an equal distribution in the three-dimensional space but do not calculate the diffusion tensor. These approaches to the resolution of multiple fibre directions in voxels are based on much more complex models of diffusion in nerve tissue (see Figs. 8.7 and 8.8).

HARDI methods can be categorized on the basis of the approach used to mathematically model the orientation dependence of the

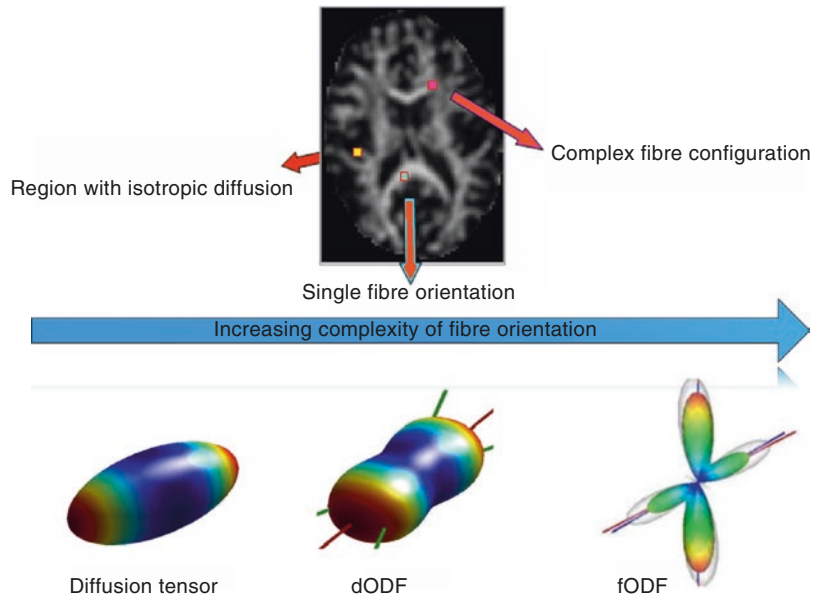

Fig. 8.8 Possible scenarios of fibre configurations in a voxel. As fibre number per voxel and orientation complexity increase, the diffusion tensor becomes less appropriate for characterizing tissue microstructure, while diffusion or fibre orientation distribution functions (dODF and fODF) provide better performances

diffusion-weighted MR signal. Estimates of fibre orientation are obtained either through the diffusion orientation density function (dODF) or the fibre orientation density function (fODF). The diffusion ODF is a spherical function that, for any point on the sphere, represents the relative number of particles that have diffused along the axis joining that point to the origin. In the case of co-axial fibres, the dODF can be used to infer the orientation of the fibres. However, the dODF will be non-zero in all other directions, since water can also diffuse perpendicular to the fibre direction (albeit hardly). In general, dODF approaches require reconstruction of the diffusion propagator, i.e. the density of the probability that a particle has moved a certain distance within the diffusion time. In principle, and taking into account the limits of acquisition time, these models do not require uncertain model assumptions to be made, which instead needed in fODF methods. However, an implicit modelling does exist in order to make any inferences, and it regards the relationship between the diffusion propagator and the microstructural properties of the tissue of interest (e.g. fibre bundle directions or partial volume). Despite dODF advantages, the exact reconstruction of the entire diffusion propagator is not achievable in practice, due to the limits of most acquisition schemes, which foresee a single *b* value. In such cases, substantial modelling simplifications must be invoked, the most common of which is DTI itself. Reconstructing the diffusion ODF is the aim of approaches such as diffusion spectrum imaging [64] and Q-ball imaging [65]. The original version of the latter had some issues related to spherical coordinates, which have been taken into account in subsequent developments of the method [66, 67], referred to as constant solid angle Q-ball imaging. Other models that employ dODF are multi-compartment models, which extend the single DTI model by summing up the contributions of multiple tensors [68]. Multi-compartment models are currently used in probabilistic tractography on DTI data [44, 45].

The composite hindered and restricted model of diffusion (CHARMED) method [69] combines elements of DTI and Q-ball imaging, thus simultaneously accounting for hindered diffusion in the extracellular space and within cell bodies and for restricted diffusion in the intra-axonal space, respectively. Hindered diffusion is modelled by a diffusion tensor, while restricted diffusion requires special solutions for a cylindrical restricted diffusion space. The parameters of the model need to be estimated from measurements at both low and high *b* values.

In contrast to diffusion propagator and dODF approaches, which essentially describe the diffusion within a voxel, fibre ODF techniques aim at estimating relative fibre density over orientation space. In the case of all fibres being parallel to the x-axis, for example, the true fODF will be a delta function pointing along the x-axis and zero in all other orientations. In this case, only the angular distribution of fibre orientations is inferred from the angular structure of either the signal [70] or of the dODF [20] by spherical deconvolution with a kernel. This kernel is essentially the simplest model of the diffusion properties of a single fibre that the data support (e.g. white matter with the highest anisotropy must contain a single-fibre orientation).

Despite many aspects of the white matter (e.g. axon diameter and packing density) may vary across brain regions, the single-fibre response will only be an approximation that is generalized across the brain. However, fODFs are superior to dODFs with respect to angular resolution and precision.

Reconstructing the fODF is the aim of approaches such as spherical deconvolution [70–74].

Many tract-reconstruction algorithms exploit peaks in the dODF or fODF to propagate white matter trajectories.

It should be emphasized that, even using HARDI techniques, none of these methods is capable of reconstructing nerve fibres or even fibre bundles. As what happens in the case of DTI data, tractography only computes trajectories or pathways through the data, to which a large portion of the nerve fibres should reasonably run in parallel.

The degree of anisotropy can also be estimated directly using HARDI methods without calculating the tensor. In this case, an anisotropy index, the spherical diffusion variance, is used instead of conventional FA. Given that, unlike the tensor, this method is not based on an a priori physical model of diffusion, it has the advantage of not losing any information contained in the data. HARDI and its future developments appear to be very promising, and the evolution of tractography is likely to be based on it even though it requires specialized acquisition sequences, generally longer acquisition times than tensor methods, more complex processing algorithms and, save for *q*-ball imaging, very powerful gradients [40].

8.4.4 Error Correction Methods

Tractography may yield anatomical reconstruction errors with any technique. These errors can be minimized using one of two methods of result analysis, one based on functional brain anatomy and one, a probabilistic method, using a standard space of brain coordinates. The first consists of using the anatomical data a priori by requiring a fibre tract to pass through at least two manually selected regions of interest (ROIs) [60, 75]. Using a single ROI, the reconstructed tract is more likely to contain different fibres, some representing trajectories belonging to the tract being studied and others generated by partial volume effects or noise. The latter can be eliminated by selecting multiple ROIs along the fibre tract being reconstructed so as to avoid an erroneous deviation of the reconstruction algorithm from the actual trajectory (Fig. 8.9). This method makes it possible to track simply and non-invasively the position of several tracts with a high level of confidence [60, 75]. Its main drawback is that it cannot reconstruct bundles that are not well documented anatomically [75] and may also exhibit limitations in the presence of fibre deviations induced by brain disease.

The second probabilistic method is based on the assumption that errors induced by partial volume effects or low SNR have a random distribution and are not reproduced consistently if multiple studies of the same object are performed, and their results are superimposed. The same principle underpins a method that uses data from a large sample of subjects in a standard space of brain coordinates (e.g. the Talairach atlas). The first studies applying this method of normalization have yielded a high level of reproducibility for the large fibre bundles, but greater intersubject variability for the smaller bundles [39, 76–78].

8.4.5 The Problem of Validation

One of the critical problems in the development of fibre-tracking techniques is that there are no other available methods to assess the course of nerve fibres in vivo or reference standards to which data can be compared. Indeed, knowledge of white matter fibre anatomy derives from post-mortem studies, where even in the best conditions only the main fibre bundles can be followed and the resolution is insufficient to constitute a reference for validation [75].

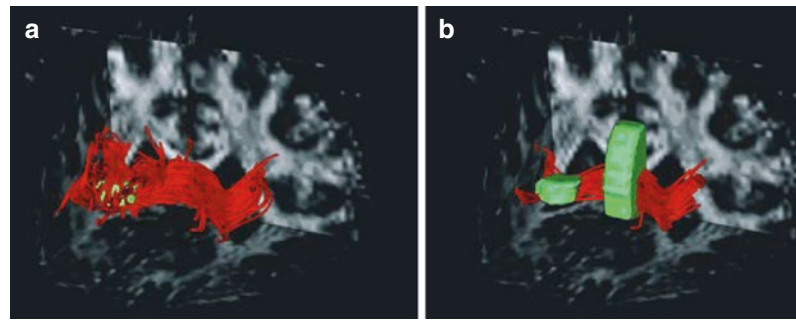

Fig. 8.9 (**a**, **b**) The use of the multi-ROI approach improves tractographic reconstruction of white matter tracts. Above, the addition of a second ROI (**b**) specifically selects the fibre tract of interest

Ablation studies of animal models make it possible to document the course of axons using specific tracers. Though representing the reference standard for connectivity studies, these data cannot, however, be extended to humans because tracer methods follow single axons at the cell level, and axons may cross different fibre bundles along their course. Owing to the practical impossibility of obtaining adequate statistics for 10^{11} neurons, these methods cannot be used to validate effectively data obtained using tractographic techniques.

Despite the limitations outlined above, a good agreement between fibre tracking and anatomy has, however, been demonstrated [39, 76].

Another limitation for DTI-derived results validation is related not only to inter-scanner differences, but also to intra-scanner variability, meaning that diffusion tensor estimation, and subsequent fibre tracking, might be heavily influenced by slight differences even for the same subject undergoing the same MRI protocol at two different times [79]. Estimation of variability sources is currently being addressed also thanks to large, publicly available databases, such as the Alzheimer's Disease Neuroimaging Initiative [80] and the Parkinson's Progression Markers Initiative [81], which provide high-quality MRI data acquired on different scanners, from both patients and healthy subjects and at multiple timepoints. These databases represent a precious resource in order to identify and address those variability sources that largely influence tractography results.

8.5 Clinical Applications

The potential clinical applications of tractographic techniques are numerous [82, 83], first and foremost in physiological studies of human CNS, where they enable in vivo identification of the topographic distribution of circuits shown by anatomical primate research and surmised in man.

In neurophysiology, tractography has fostered the development of a new strategy to study brain activity patterns: anatomical connectivity. This technique is based on the possibility of visualizing directly the connections among the brain areas activated during a given task and conceptually complements two other strategies that explore connectivity, i.e. functional connectivity (the study of how two cerebral areas tend to work in a correlated manner) and effective connectivity (the study of the information flow within an active pattern by identifying its direction and orientation). Anatomical connectivity is essential, because it provides evidence for the existence of anatomical connections, which are indispensable elements to confirm and validate the results of functional and effective connectivity studies. An example is the study of the connectivity of the dopaminergic system, which originates in substantia nigra neurons in the pars compacta of the mesencephalon. Tractography has recently made it possible to identify the course of human dopaminergic fibres as far as the corpus striatum (nigrostriatal circuit) and their subsequent cortical distribution (corticostriatal circuit) [84] (Fig. 8.10).

The use of this method in neurological investigations is obvious, especially in degenerative CNS disease. In Parkinson's disease, MR has a limited role except in the differential diagnosis from other diseases, since its diagnosis is essentially clinical but can only be confirmed by post-mortem histopathological examination. By identifying the dopaminergic fibres at their origin, tractography can quantify the axonal depletion and thus provide an index of disease severity. Another common degenerative disease, Alzheimer's, is characterized already in its early phase by a depletion of temporo-mesial neurons, which can be identified with tractography [85–93]. In Huntington's disease, a neurodegenerative autosomal dominate disorder, MR tractography has shown white matter abnormalities prior to the disease onset [94–96].

In neurophysiology, electrophysiological data – indirect indicators of fibre integrity – could be better interpreted using tractography, which is capable of displaying fibre tracts directly. For instance, corticospinal fibres can be identified and reconstructed with tractography from their

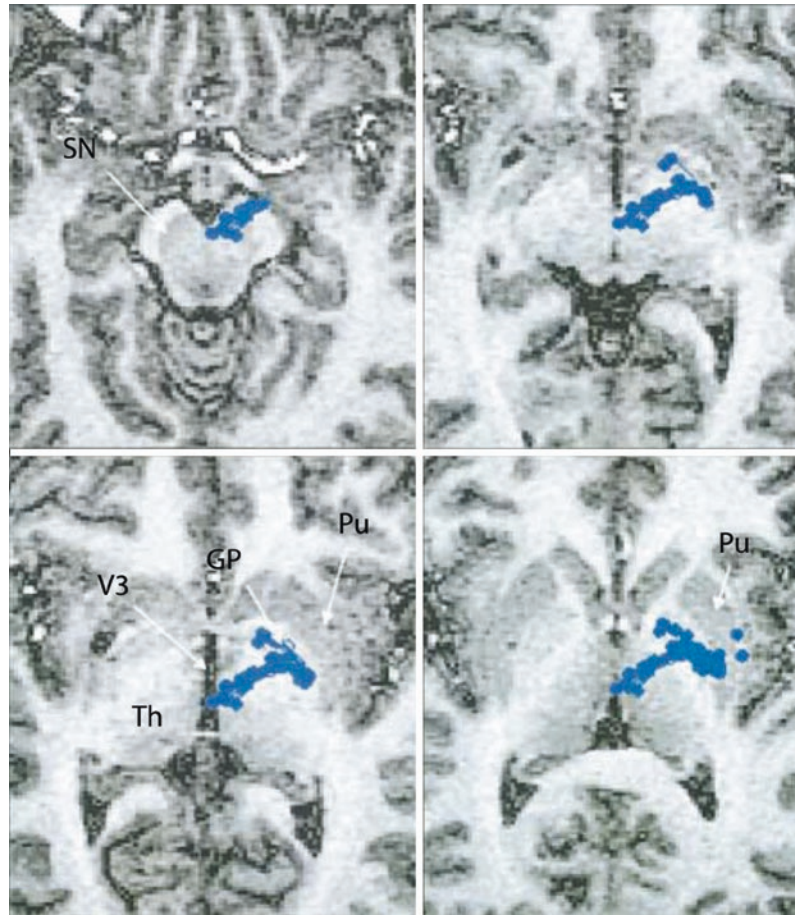

Fig. 8.10 T1-weighted axial images at the level of the mesencephalon (*upper left*), subthalamic area (*upper right*) and thalamus (*lower left and right*). *Blue points* represent the fibre tract reconstructed from the putamen through globus pallidus, subthalamic area and medial substantia nigra. *GP* globus pallidus, *Pu* putamen, *SN* substantia nigra, *Th* thalamus, *V3* third ventricle (Image from Lehéricy et al. [84])

origin through the centrum semiovale, corona radiata, internal capsule and cerebral peduncle. Identification of this bundle is important in neurological diseases like multiple sclerosis, where demyelination and the consequent axon damage even at a distance from the lesion site can be documented and quantified using these techniques [97–112].

In neurosurgery, knowledge of the course of nerve fibre bundles (Fig. 8.11) and their relationships to the expanding lesion can preserve them from resection [113–123].

Another application of tractography in this field is represented by connectivity-based classification of a seed region. As the name suggests, this method classifies each voxel of the starting region for tractography on the basis of the region of the brain to which it connects with the highest probability. For example, it has been applied to identify areas of the basal ganglia connected to different cortical regions, both in healthy subjects and Parkinson's disease patients [124, 125]. Connectivity-based classification could also be used before and after surgery, in order to assess changes in the connectivity of the region near the surgical breach towards the rest of the brain.

Finally, tractography should be applied to identify and describe the brain plasticity phenomena secondary to CNS lesions. Identification of the axonal loss and consequent impairment of further adjacent or distant circuits, normally not involved in a given function, can offer insights into the complex phenomena underpinning clinical recovery and enable better targeted pharmacological and rehabilitation therapy [126–138].

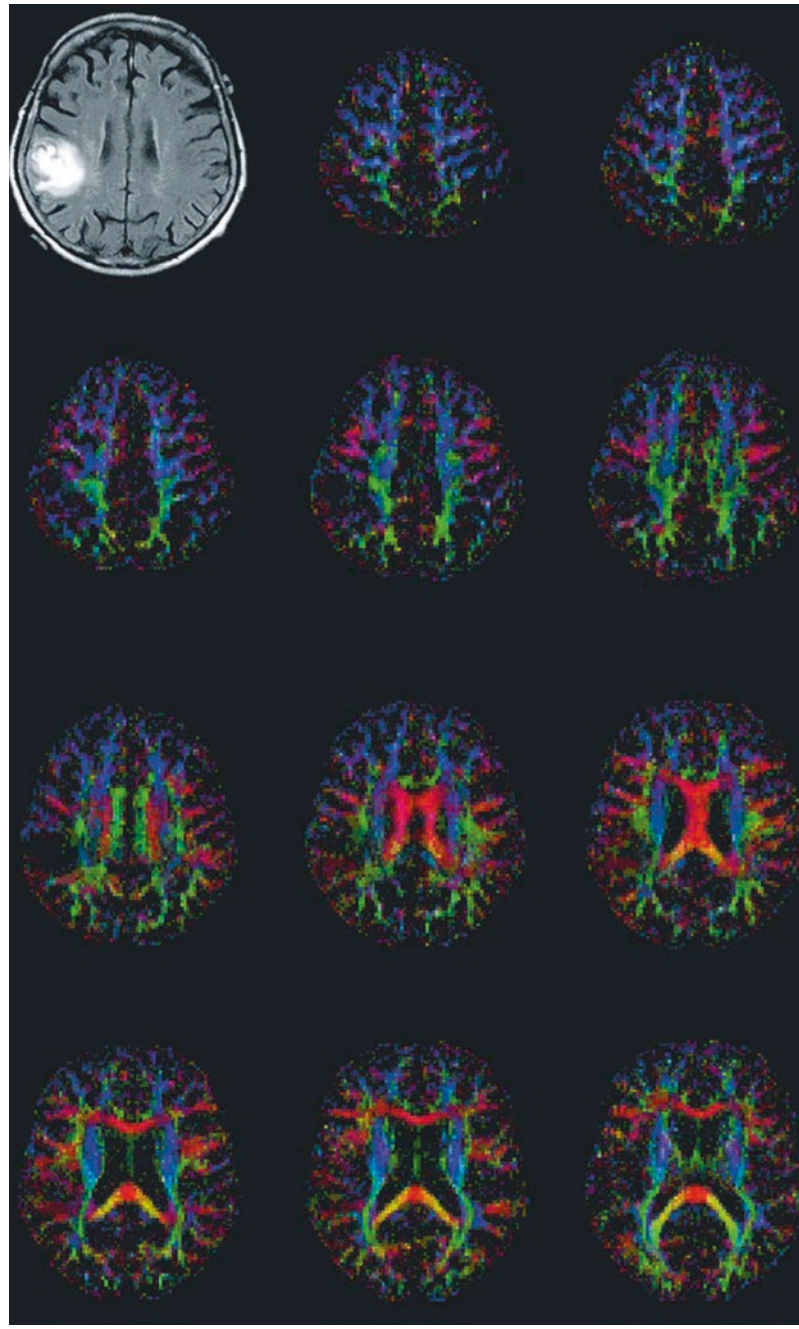

Fig. 8.11 Axial FLAIR image (*upper left*) compared with fractional anisotropy maps. DTI-based colour orientation map: *red* = *x* direction; *green* = *y* direction; *blue* = *z* direction. A tumour shown in the FLAIR image alters the course of surrounding fibres in several slices, as shown by the DTI data

Conclusion

We have described the main MR tractographic techniques, which enable in vivo and non-invasive reconstruction of the anatomy of axon fibres, documenting the connections among grey matter areas. Tractography is the natural complement of functional MR, which can depict the activation of these areas. Combined use of these techniques is expected to be performed with increasing frequency in

the future [118, 121, 139, 140], and to yield useful results in the study of physiological and pathological CNS mechanisms, enabling better planning and quantification of therapeutic interventions.

References

1. Basser PJ, Jones DK (2002) Diffusion-tensor MRI: theory, experimental design and data analysis – a technical review. NMR Biomed 15:456–467
2. Basser PJ, Pajevic S, Pierpaoli C et al (2000) In vivo fiber tractography using DT-MRI data. Magn Reson Med 44:625–632
3. Bammer R, Acar B, Moseley ME (2003) In vivo MR tractography using diffusion imaging. Eur J Radiol 45:223–234
4. Mori S, van Zijl PC (2002) Fiber tracking: principles and strategies – a technical review. NMR Biomed 15:468–480
5. Habas C (2004) Basic principles of diffusion tensor MR tractography. J Radiol 85:281–286
6. Conturo TE, Lori NF, Cull TS et al (1999) Tracking neuronal fiber pathways in the living human brain. Proc Natl Acad Sci U S A 96:10422–10427
7. Beaulieu C (2002) The basis of anisotropic water diffusion in the nervous system – a technical review. NMR Biomed 15:435–455
8. Moseley ME, Cohen Y, Kucharczyk J et al (1990) Diffusion-weighted MR imaging of anisotropic water diffusion in cat central nervous system. Radiology 176:439–445
9. Le Bihan D, Mangin JF, Poupon C et al (2001) Diffusion tensor imaging: concepts and applications. J Magn Reson Imaging 13:534–546
10. Basser PJ, Mattiello J, LeBihan D (1994) MR diffusion tensor spectroscopy and imaging. Biophys J 66:259–267
11. Basser PJ, Mattiello J, LeBihan D (1994) Estimation of the effective self-diffusion tensor from the NMR spin echo. J Magn Reson B 103:247–254
12. Batchelor PG, Moakher M, Atkinson D et al (2005) A rigorous framework for diffusion tensor calculus. Magn Reson Med 53:221–225
13. Parker GJ (2004) Analysis of MR diffusion weighted images. Br J Radiol 77 Spec No 2:S176–S185
14. Lori NF, Akbudak E, Shimony JS et al (2002) Diffusion tensor fiber tracking of human brain connectivity: acquisition methods, reliability analysis and biological results. NMR Biomed 15:494–515
15. Assaf Y, Freidlin RZ, Rohde GK et al (2004) New modeling and experimental framework to characterize hindered and restricted water diffusion in brain white matter. Magn Reson Med 52:965–978
16. Nagae-Poetscher LM, Jiang H, Wakana S et al (2004) High-resolution diffusion tensor imaging of the brain stem at 3 T. AJNR 25:1325–1330
17. Burdette JH, Elster AD, Ricci PE (1998) Calculation of apparent diffusion coefficients (ADCs) in brain using two-point and six-point methods. J Comput Assist Tomogr 22:792–794
18. Xing D, Papadakis NG, Huang CL et al (1997) Optimised diffusion weighting for measurement of apparent diffusion coefficient (ADC) in human brain. Magn Reson Imaging 15:771–784
19. Melhem ER, Mori S, Mukundan G et al (2002) Diffusion tensor MR imaging of the brain and white matter tractography. AJR 178:3–16
20. Descoteaux M, Deriche R, Knösche TR, Anwander A (2009) Deterministic and probabilistic tractography based on complex fibre orientation distributions. IEEE Trans Med Imaging 28:269–286
21. Jeurissen B, Leemans A, Tournier J-D et al (2012) Investigating the prevalence of complex fiber configurations in white matter tissue with diffusion magnetic resonance imaging. Hum Brain Mapp 34(11):2747–2766
22. Jones DK (2004) The effect of gradient sampling schemes on measures derived from diffusion tensor MRI: a Monte Carlo study. Magn Reson Med 51: 807–815
23. Daducci A, Canales-Rodriguez EJ, Descoteaux M et al (2013) Quantitative comparison of reconstruction methods for intra-voxel fiber recovery from diffusion MRI. IEEE Trans Med Imaging 33(2): 384–399
24. Griswold MA, Jakob PM, Heidemann RM et al (2002) Generalized autocalibrating partially parallel acquisitions (GRAPPA). Magn Reson Med 47: 1202–1210
25. Setsompop K, Cohen-Adad J, Gagoski BA et al (2012) Improving diffusion MRI using simultaneous multi-slice echo planar imaging. Neuroimage 63(1): 569–580
26. Paley MN, Lee KJ, Wild JM et al (2006) Simultaneous parallel inclined readout image technique. Magn Reson Imaging 24:557–562
27. Weaver JB (1988) Simultaneous multislice acquisition of MR images. Magn Reson Med 8:275–284
28. Feinberg DA, Reese TG, Wedeen VJ (2002) Simultaneous echo refocusing in EPI. Magn Reson Med 48:1–5
29. Reese TG, Benner T, Wang R et al (2009) Halving imaging time of whole brain diffusion spectrum imaging and diffusion tractography using simultaneous image refocusing in EPI. J Magn Reson Imaging 29:517–522
30. Breuer FA, Blaimer M, Heidemann RM et al (2005) Controlled aliasing in parallel imaging results in higher acceleration (CAIPIRINHA) for multi-slice imaging. Magn Reson Med 53:684–691
31. Larkman DJ, Hajnal JV, Herlihy AH et al (2001) Use of multicoil arrays for separation of signal from multiple slices simultaneously excited. J Magn Reson Imaging 13:313–317
32. Moeller S, Yacoub E, Olman CA et al (2010) Multiband multislice GE-EPI at 7 tesla, with 16-fold

acceleration using partial parallel imaging with application to high spatial and temporal whole-brain fMRI. Magn Reson Med 63:1144–1153
33. Nunes RG, Hajnal JV, Golay X, et al. (2006) Simultaneous slice excitation and reconstruction for single shot EPI. Proceedings of the 14th Annual Meeting of ISMRM, Seattle, p. 293
34. Setsompop K, Gagoski BA, Polimeni J et al (2012) Blipped-controlled aliasing in parallel imaging (blipped-CAIPI) for simultaneous multi-slice EPI with reduced g-factor penalty. Magn Reson Med 67:1210–1224
35. Xue R, van Zijl PC, Crain BJ et al (1999) In vivo three-dimensional reconstruction of rat brain axonal projections by diffusion tensor imaging. Magn Reson Med 42:1123–1127
36. Mori S, Crain BJ, Chacko VP et al (1999) Three-dimensional tracking of axonal projections in the brain by magnetic resonance imaging. Ann Neurol 45:265–269
37. Parker GJ, Stephan KE, Barker GJ et al (2002) Initial demonstration of in vivo tracing of axonal projections in the macaque brain and comparison with the human brain using diffusion tensor imaging and fast marching tractography. Neuroimage 15:797–809
38. Parker GJ, Wheeler-Kingshott CA, Barker GJ (2002) Estimating distributed anatomical connectivity using fast marching methods and diffusion tensor imaging. IEEE Trans Med Imaging 21:505–512
39. Ciccarelli O, Toosy AT, Parker GJ et al (2003) Diffusion tractography based group mapping of major white-matter pathways in the human brain. Neuroimage 19:1545–1555
40. Duncan JS, Papademetris X, Yang J et al (2004) Geometric strategies for neuroanatomic analysis from MRI. Neuroimage 23(1):S34–S45
41. Wu YC, Field AS, Chung MK et al (2004) Quantitative analysis of diffusion tensor orientation: theoretical framework. Magn Reson Med 52: 1146–1155
42. Parker GJ, Alexander DC (2003) Probabilistic Monte Carlo based mapping of cerebral connections utilising whole-brain crossing fibre information. Inf Process Med Imaging 18:684–695
43. Parker GJ, Haroon HA, Wheeler-Kingshott CA (2003) A framework for a streamline-based probabilistic index of connectivity (PICo) using a structural interpretation of MRI diffusion measurements. J Magn Reson Imaging 18:242–254
44. Behrens TE, Woolrich MW, Jenkinson M et al (2003) Characterization and propagation of uncertainty in diffusion-weighted MR imaging. Magn Reson Med 50:1077–1088
45. Behrens TE, Berg HJ, Jbabdi S et al (2007) Probabilistic diffusion tractography with multiple fibre orientations: what can we gain? Neuroimage 34(1):144–155
46. Filippi M, van den Heuvel MP, Fornito A et al (2013) Assessment of system dysfunction in the brain through MRI-based connectomics. Lancet Neurol 12:1189–1199
47. de Schotten MT, Ffytche DH, Bizzi A et al (2011) Atlasing location, asymmetry and inter-subject variability of white matter tracts in the human brain with MR diffusion tractography. Neuroimage 54(1): 49–59
48. Hagmann P (2005) From diffusion MRI to brain connectomics. Signal Processing Institute. Ecole Polytechnique Fédérale de Lausanne (EPFL). Lausanne, p 127. doi:10.5075/epfl-thesis-3230
49. Sporns O, Tononi G, Kotter R (2005) The human connectome: a structural description of the human brain. PLoS Comput Biol 1:e42
50. Bullmore E, Sporns O (2009) Complex brain networks: graph theoretical analysis of structural and functional systems. Nat Rev Neurosci 10(3):186–198
51. Wen W, Zhu WL, He Y et al (2011) Discrete neuroanatomical networks are associated with specific cognitive abilities in old age. J Neurosci 31(4):1204–1212
52. Bernhardt BC, Bonilha L, Gross DW (2015) Network analysis for a network disorder: the emerging role of graph theory in the study of epilepsy. Epilepsy Behav 50:162–170
53. Griffa A, Baumann PS, Thiran J-P et al (2013) Structural connectomics in brain diseases. Neuroimage 80:515–526
54. Korgaonkar MS, Fornito A, Williams LM et al (2014) Abnormal structural networks characterize major depressive disorder: a connectome analysis. Biol Psychiatry 76:567–574
55. Phillips DJ, McGlaughlin A, Ruth D et al (2015) Graph theoretic analysis of structural connectivity across the spectrum of Alzheimer's disease: the importance of graph creation methods. NeuroImage Clin 7:377–390
56. Jones DK, Basser PJ (2004) "Squashing peanuts and smashing pumpkins": how noise distorts diffusion-weighted MR data. Magn Reson Med 52:979–993
57. Jones DK (2003) Determining and visualizing uncertainty in estimates of fiber orientation from diffusion tensor MRI. Magn Reson Med 49:7–12
58. Anderson AW (2001) Theoretical analysis of the effects of noise on diffusion tensor imaging. Magn Reson Med 46:1174–1188
59. Lazar M, Weinstein DM, Tsuruda JS et al (2003) White matter tractography using diffusion tensor deflection. Hum Brain Mapp 18:306–321
60. Huang H, Zhang J, van Zijl PC et al (2004) Analysis of noise effects on DTI-based tractography using the brute-force and multi-ROI approach. Magn Reson Med 52:559–565
61. Heim S, Hahn K, Samann PG et al (2004) Assessing DTI data quality using bootstrap analysis. Magn Reson Med 52:582–589
62. Alexander AL, Hasan KM, Lazar M et al (2001) Analysis of partial volume effects in diffusion-tensor MRI. Magn Reson Med 45:770–780
63. Barrick TR, Clark CA (2004) Singularities in diffusion tensor fields and their relevance in white matter fiber tractography. Neuroimage 22:481–491
64. Wedeen VJ, Hagmann P, Tseng WYI et al (2005) Mapping complex tissue architecture with diffusion

spectrum magnetic resonance imaging. Magn Reson Med 54:1377–1386
65. Tuch DS (2004) Q-ball imaging. Magn Reson Med 52:1358–1372
66. Tristán-Vega A, Westin C-F, Aja-Fernández S (2009) Estimation of fiber orientation density probability density functions in high angular resolution diffusion imaging. Neuroimage 47:638–650
67. Aganj I, Lenglet C, Sapiro E et al (2010) Reconstruction of the orientation distribution function in single and multiple shell q-ball imaging with constant solid angle. Magn Reson Med 64:554–566
68. Liu C, Bammer R, Acar B et al (2004) Characterizing non-Gaussian diffusion by using generalized diffusion tensors. Magn Reson Med 51:924–937
69. Assaf Y, Basser P (2005) Composite hindered and restricted model of diffusion (charmed) MR imaging of the human brain. Neuroimage 27:48–58
70. Tournier JD, Calamante F, Gadian DG et al (2004) Direct estimation of the fiber orientation density function from diffusion-weighted MRI data using spherical deconvolution. Neuroimage 23:1176–1185
71. Alexander DC, (2005) Maximum entropy spherical deconvolution for diffusion MRI. In: Christensen GE, Soka M (eds) Information processing in medical imaging, proceedings, pp 76–87
72. Dell'Acqua F, Scifo P, Rizzo G et al (2010) A modified damped Richardson–Lucy algorithm to reduce isotropic background effects in spherical deconvolution. Neuroimage 49:1446–1458
73. Kaden E, Knösche TR, Anwander A (2007) Parametric spherical deconvolution: inferring anatomical connectivity using diffusion MR imaging. Neuroimage 37:474–488
74. Patel V, Shi Y, Thompson PM et al (2010) Mesh-based spherical deconvolution: a flexible approach to reconstruction of non-negative fiber orientation distributions. Neuroimage 51:1071–1081
75. Mori H, Masutani Y, Aoki S et al (2003) Simple visualization of the corticospinal pathway using tractography: one-ROI and two-ROI methods. Nippon Igaku Hoshasen Gakkai Zasshi 63:51–53
76. Ciccarelli O, Parker GJ, Toosy AT et al (2003) From diffusion tractography to quantitative white matter tract measures: a reproducibility study. Neuroimage 18:348–359
77. Catani M, Jones DK, Donato R et al (2003) Occipito-temporal connections in the human brain. Brain 126:2093–2107
78. Holodny AI, Gor DM, Watts R et al (2005) Diffusion-tensor MR tractography of somatotopic organization of corticospinal tracts in the internal capsule: initial anatomic results in contradistinction to prior reports. Radiology 234:649–653
79. Lemkaddem A, Daducci A, Vulliemoz S et al (2012) A multi-center study: intra-scan and inter-scan variability of diffusion spectrum imaging. Neuroimage 62(1):87–94
80. Jack CR, Bernstein MA, Fox NC et al (2008) The Alzheimer's Disease Neuroimaging Initiative (ADNI): MRI methods. J Magn Reson Imaging JMRI 27(4):685–691
81. Marek K, Jennings D, Lasch S et al (2011) The Parkinson Progression Marker Initiative (PPMI). Prog Neurobiol 95(4):629–635
82. Oppenheim C, Rodrigo S, Poupon C et al (2004) Diffusion tensor MR imaging of the brain. Clinical applications. J Radiol 85:287–296
83. Sundgren PC, Dong Q, Gomez-Hassan D et al (2004) Diffusion tensor imaging of the brain: review of clinical applications. Neuroradiology 46:3 39–350
84. Lehericy S, Ducros M, Van de Moortele PF et al (2004) Diffusion tensor fiber tracking shows distinct corticostriatal circuits in humans. Ann Neurol 55:522–529
85. Rose SE, Chen F, Chalk JB et al (2000) Loss of connectivity in Alzheimer's disease: an evaluation of white matter tract integrity with colour coded MR diffusion tensor imaging. J Neurol Neurosurg Psychiatry 69:528–530
86. Bozzali M, Franceschi M, Falini A et al (2001) Quantification of tissue damage in AD using diffusion tensor and magnetization transfer MRI. Neurology 57:1135–1137
87. Bozzali M, Falini A, Franceschi M et al (2002) White matter damage in Alzheimer's disease assessed in vivo using diffusion tensor magnetic resonance imaging. J Neurol Neurosurg Psychiatry 72:742–746
88. Horsfield MA, Jones DK (2002) Applications of diffusion weighted and diffusion tensor MRI to white matter diseases – a review. NMR Biomed 15:570–577
89. Larsson EM, Englund E, Sjobeck M et al (2004) MRI with diffusion tensor imaging post-mortem at 3.0 T in a patient with frontotemporal dementia. Dement Geriatr Cogn Disord 17:316–319
90. Sugihara S, Kinoshita T, Matsusue E et al (2004) Usefulness of diffusion tensor imaging of white matter in Alzheimer disease and vascular dementia. Acta Radiol 45:658–663
91. Sun Y, Du XK, Zhang ZX et al (2004) Relationship between the data from MR-diffusion tensor imaging and the clinical cognitive evaluation in Alzheimer's disease. Zhongguo Yi Xue Ke Xue Yuan Xue Bao 26:134–138
92. Yoshida T, Shiga K, Yoshikawa K et al (2004) White matter loss in the splenium of the corpus callosum in a case of posterior cortical atrophy: a diffusion tensor imaging study. Eur Neurol 52:77–81
93. Sullivan EV, Pfefferbaum A (2003) Diffusion tensor imaging in normal aging and neuropsychiatric disorders. Eur J Radiol 45:244–255
94. Phillips O, Sanchez-Castaneda C, Elifani F et al (2013) Tractography of the corpus callosum in Huntington's disease. PLoS One 8:1–9
95. Phillips O, Squitieri F, Sanchez-Castaneda C et al (2014) Deep white matter in Huntington's disease. PLoS One 23(9):10

96. Phillips O, Squitieri F, Sanchez-Castaneda C et al (2015) The cortispinal tract in Huntington's disease. Cereb Cortex 25(9):2670–2682
97. Rovaris M, Gallo A, Valsasina P et al (2005) Short-term accrual of gray matter pathology in patients with progressive multiple sclerosis: an in vivo study using diffusion tensor MRI. Neuroimage 24:1139–1146
98. Hong YH, Lee KW, Sung JJ et al (2004) Diffusion tensor MRI as a diagnostic tool of upper motor neuron involvement in amyotrophic lateral sclerosis. J Neurol Sci 227:73–78
99. Yin H, Lim CC, Ma L et al (2004) Combined MR spectroscopic imaging and diffusion tensor MRI visualizes corticospinal tract degeneration in amyotrophic lateral sclerosis. J Neurol 251:1249–1254
100. Abe O, Yamada H, Masutani Y et al (2004) Amyotrophic lateral sclerosis: diffusion tensor tractography and voxel-based analysis. NMR Biomed 17:411–416
101. Cassol E, Ranjeva JP, Ibarrola D et al (2004) Diffusion tensor imaging in multiple sclerosis: a tool for monitoring changes in normal-appearing white matter. Mult Scler 10:188–196
102. Ulug AM, Grunewald T, Lin MT et al (2004) Diffusion tensor imaging in the diagnosis of primary lateral sclerosis. J Magn Reson Imaging 19:34–39
103. Rashid W, Hadjiprocopis A, Griffin CM et al (2004) Diffusion tensor imaging of early relapsing-remitting multiple sclerosis with histogram analysis using automated segmentation and brain volume correction. Mult Scler 10:9–15
104. Sach M, Winkler G, Glauche V et al (2004) Diffusion tensor MRI of early upper motor neuron involvement in amyotrophic lateral sclerosis. Brain 127:340–350
105. Ciccarelli O, Werring DJ, Barker GJ et al (2003) A study of the mechanisms of normal-appearing white matter damage in multiple sclerosis using diffusion tensor imaging – evidence of Wallerian degeneration. J Neurol 250:287–292
106. Cercignani M, Bozzali M, Iannucci G et al (2002) Intravoxel and inter-voxel coherence in patients with multiple sclerosis assessed using diffusion tensor MRI. J Neurol 249:875–883
107. Tench CR, Morgan PS, Wilson M et al (2002) White matter mapping using diffusion tensor MRI. Magn Reson Med 47:967–972
108. Guo AC, MacFall JR, Provenzale JM (2002) Multiple sclerosis: diffusion tensor MR imaging for evaluation of normal appearing white matter. Radiology 222:729–736
109. Filippi M, Rocca MA, Falini A et al (2002) Correlations between structural CNS damage and functional MRI changes in primary progressive MS. Neuroimage 15:537–546
110. Assaf Y, Ben-Bashat D, Chapman J et al (2002) High b-value q-space analyzed diffusion-weighted MRI: application to multiple sclerosis. Magn Reson Med 47:115–126
111. Horsfield MA, Larsson HB, Jones DK et al (1998) Diffusion magnetic resonance imaging in multiple sclerosis. J Neurol Neurosurg Psychiatry 64(1):S80–S84
112. Castriota-Scanderbeg A, Tomaiuolo F, Sabatini U et al (2000) Demyelinating plaques in relapsing-remitting and secondary-progressive multiple sclerosis: assessment with diffusion MR imaging. AJNR 21:862–868
113. Nimsky C, Ganslandt O, Hastreiter P et al (2005) Intraoperative diffusion-tensor MR imaging: shifting of white matter tracts during neurosurgical procedures – initial experience. Radiology 234:218–225
114. Wu JS, Zhou LF, Hong XN et al (2003) Role of diffusion tensor imaging in neuronavigation surgery of brain tumors involving pyramidal tracts. Zhonghua Wai Ke Za Zhi 41:662–666
115. Clark CA, Barrick TR, Murphy MM et al (2003) White matter fiber tracking in patients with space-occupying lesions of the brain: a new technique for neurosurgical planning? Neuroimage 20:1601–1608
116. Akai H, Mori H, Aoki S et al (2005) Diffusion tensor tractography of gliomatosis cerebri: fiber tracking through the tumor. J Comput Assist Tomogr 29:127–129
117. Nimsky C, Ganslandt O, Hastreiter P et al (2005) Preoperative and intraoperative diffusion tensor imaging-based fiber tracking in glioma surgery. Neurosurgery 56:130–138
118. Parmar H, Sitoh YY, Yeo TT (2004) Combined magnetic resonance tractography and functional magnetic resonance imaging in evaluation of brain tumors involving the motor system. J Comput Assist Tomogr 28:551–556
119. Kier EL, Staib LH, Davis LM et al (2004) MR imaging of the temporal stem: anatomic dissection tractography of the uncinate fasciculus, inferior occipitofrontal fasciculus, and Meyer's loop of the optic radiation. AJNR 25:677–691
120. Barboriak DP (2003) Imaging of brain tumors with diffusion-weighted and diffusion tensor MR imaging. Magn Reson Imaging Clin N Am 11:379–401
121. Guye M, Parker GJ, Symms M et al (2003) Combined functional MRI and tractography to demonstrate the connectivity of the human primary motor cortex in vivo. Neuroimage 19:1349–1360
122. Holodny AI, Ollenschlager M (2002) Diffusion imaging in brain tumors. Neuroimaging Clin N Am 12:107–124
123. Holodny AI, Schwartz TH, Ollenschleger M et al (2001) Tumor involvement of the corticospinal tract: diffusion magnetic resonance tractography with intraoperative correlation. J Neurosurg 95:1082
124. Leh SE, Ptito A, Chakravarty MM et al (2007) Fronto-striatal connections in the human brain: a probabilistic diffusion tractography study. Neurosci Lett 419:113–118
125. Sharman M, Valabregue R, Perlbarg V et al (2013) Parkinson's disease patients show reduced cortical-

subcortical sensorimotor connectivity. Mov Disord 28(4):447–454
126. Le TH, Mukherjee P, Henry RG et al (2005) Diffusion tensor imaging with three-dimensional fiber tractography of traumatic axonal shearing injury: an imaging correlate for the posterior callosal "disconnection" syndrome: case report. Neurosurgery 56:189
127. Naganawa S, Sato C, Ishihra S et al (2004) Serial evaluation of diffusion tensor brain fiber tracking in a patient with severe diffuse axonal injury. AJNR 25:1553–1556
128. Huisman TA, Schwamm LH, Schaefer PW et al (2004) Diffusion tensor imaging as potential biomarker of white matter injury in diffuse axonal injury. AJNR 25:370–376
129. Huisman TA, Sorensen AG, Hergan K et al (2003) Diffusion-weighted imaging for the evaluation of diffuse axonal injury in closed head injury. J Comput Assist Tomogr 27:5–11
130. Arfanakis K, Haughton VM, Carew JD et al (2002) Diffusion tensor MR imaging in diffuse axonal injury. AJNR 23:794–802
131. Konishi J, Yamada K, Kizu O et al (2005) MR tractography for the evaluation of functional recovery from lenticulostriate infarcts. Neurology 64:108–113
132. Yamada K, Ito H, Nakamura H et al (2004) Stroke patients' evolving symptoms assessed by tractography. J Magn Reson Imaging 20:923–929
133. Munoz Maniega S, Bastin ME, Armitage PA et al (2004) Temporal evolution of water diffusion parameters is different in grey and white matter in human ischaemic stroke. J Neurol Neurosurg Psychiatry 75:1714–1718
134. Thomalla G, Glauche V, Koch MA et al (2004) Diffusion tensor imaging detects early Wallerian degeneration of the pyramidal tract after ischemic stroke. Neuroimage 22:1767–1774
135. Huisman TA (2003) Diffusion-weighted imaging: basic concepts and application in cerebral stroke and head trauma. Eur Radiol 13:2283–2297
136. Kunimatsu A, Aoki S, Masutani Y et al (2003) Three-dimensional white matter tractography by diffusion tensor imaging in ischaemic stroke involving the corticospinal tract. Neuroradiology 45:532–535
137. Sotak CH (2002) The role of diffusion tensor imaging in the evaluation of ischemic brain injury – a review. NMR Biomed 15:561–569
138. Huisman TA, Hawighorst H, Benoit CH et al (2001) Diffusion weighted MRI: ischemic and traumatic injuries of the central nervous system. Radiologe 41:1038–1047
139. Johansen-Berg H, Behrens TE, Sillery E et al (2005) Functional-anatomical validation and individual variation of diffusion tractography-based segmentation of the human thalamus. Cereb Cortex 15:31–39
140. Toosy AT, Ciccarelli O, Parker GJ et al (2004) Characterizing function-structure relationships in the human visual system with functional MRI and diffusion tensor imaging. Neuroimage 21:1452–1463